Robotica (2015) volume 33, pp. 264–281. © Cambridge University Press 2014
doi:10.1017/S0263574714000332

Active disturbance rejection for walking bipedal robots using the acceleration of the upper limbs

Joshua Hill and Farbod Fahimi*

Department of Mechanical & Aerospace Engineering, UAHuntsville, Huntsville, AL 35805, USA

(Accepted January 31, 2014. First published online: February 27, 2014)

SUMMARY

A disturbance rejection controller is proposed based on the general dynamic model of 3D biped robots. For the first time, with this proposed approach, not only the Zero Moment Point (ZMP) location remains unchanged in presence of disturbances but also the longitudinal and lateral ground reaction forces and the vertical twist moment remain unchanged. This way, slipping as well as tipping is prevented by the controller. The swing phase of the robot's walking gait is considered. An integral sliding mode architecture is chosen for the disturbance rejection. The support forces and moments of the stance foot are the control outputs. The acceleration of the arm/body joints are chosen as the inputs. During the disturbance rejection, the leg joints remain at their desired trajectory. Since the leg joint trajectories are unaffected, the robot is still able to complete its step as planned, even when bounded disturbances are experienced. For simulations, the general method is applied to an 18-degree of freedom biped humanoid robot. Simulations show that the controller successfully mitigates bounded disturbances and maintains all of the support reactions extremely close to their desired values. Consequently, the shift in the position of the ZMP is negligible, and the robot foot does not slip.

KEYWORD: Bipeds; Control of robotic systems; Humanoid robots; Motion planning; Legged robots.

1. Introduction

Humanoid robots have been a topic of fascination for many researchers for decades. The characteristic bipedal gait of humanoids has, in particular, been the focus of much research. This research can be divided into two broad, yet distinct, groups: passive bipeds and active bipeds.

Passive bipeds are those that take advantage of the natural dynamics of the system and require little to no actuation to perform a walking motion.[1] Fully passive bipeds have limited practical use, as they usually rely on potential energy to walk down an incline. Many Passive Dynamic Walkers have relatively simple mechanisms. They are sensitive to initial conditions and are usually not robust enough to handle external disturbances, and are normally the focus of studies in the energy efficiency of bipedal walking gaits.[2] The research into passive bipeds has led to developments in active bipeds where the natural dynamics of the walking gait are used to reduce the consumption of energy normally required to actuate motors.[3] The focus of this paper however falls into the category of active bipeds, or those that require significant actuation to perform their gait.

The most popular methods of control for bipedal robots use the concept of Zero Moment Point (ZMP). All the external forces acting on the robot and all the inertial forces due to the motion of robot's limbs have a resultant force. The point of intersection of this resultant force and the ground surface is the ZMP. The support polygon is the area on the ground that is covered by the feet during locomotion.

It is a necessary and sufficient condition for the stable dynamic locomotion of the biped for the ZMP to remain inside the support polygon.[4] If the ZMP moves outside the support polygon, then the robot becomes unstable and begins to fall over. The first ZMP-based approach for biped walking control has the ZMP remaining inside the support polygon at all times, as defined by the desired trajectory of the biped joints. This approach has been successfully used for Manus-I,[5] and the famous

* Corresponding author. E-mail: fahimi@eng.uah.edu

Honda Asimo Robot.[6] In this approach, the ZMP location is not directly controlled by a feedback controller. Essentially, the humanoid is given a desired set of joint trajectories to accomplish a specific task. The humanoid then performs the task following the prescribed joint trajectories. Problems occur if the robot encounters an external disturbance. Due to a lack of feedback of the ZMP location, the robot is not able to react to the external disturbance. So the ZMP could move outside the support polygon. When this happens, the robot becomes unstable and falls.

The second approach is the incorporation of feedback for ZMP disturbance compensation. In these approaches, the "joint torques" or "joint trajectories" are modified in real-time to keep the ZMP within the support polygon.

One example of modifying joint "torques" is injecting a compensating torque into the ankle joint of the foot of a robot. This modification enhances ZMP control.[7] A different method is to control the angular momentum of the robot and adjust it by modifying the joint torques.[8,9]

There have been numerous methods proposed for the modification of joint trajectories for ZMP control, mostly involving modifying the position of joints. A few methods involve varying the step time, stride, or speed of the walk,[10,11] however this method can prove problematic for certain situations, such as the stepping stone problem where the biped must step on certain locations. Modification of the humanoid's trunk or waist motion has been studied,[12–14] and even exploiting the upper body's natural dynamics in its control[15] has been considered. Modification of the motion of the robot's base link of the stance leg[16] has been introduced as well.

A full dynamic model of a humanoid robot includes many complex, coupled, nonlinear equations. As a result of this, it is normal for simplified models of the robot to be used to ease the modeling burden. A common method is to model the biped as an inverted pendulum. This model has been used for a 30-degree-of-freedom (DOF) biped to manipulate the ZMP indirectly by controlling the center of gravity.[17] In order to provide a more natural walk for bipeds, a Linear Inverted Pendulum Model (LIMP) has been used to simulate a 12-DOF robot with a moving support ZMP references.[18] The moving ZMP reference results in a motion that looks more natural than a ZMP that is kept at the center of the support polygon. The robot had separate Proportional-Integral-Derivative (PID) controllers for each leg. The three-dimensional LIMP (3D-LIPM) developed by Kajita *et al.*[19] is implemented in Lee *et al*.[20] on a 27-DOF HanSaRam-VII robot. In that work, the legs of the robot are modeled as weightless, telescopic limbs, with the mass concentrated at a single point, and the ZMP is controlled via the control of the center of gravity.

Methods that modify the acceleration of joints have been the focus of study in recent years. Maintaining the upper-body task specifications by controlling the ZMP via modifying the torso's acceleration was proposed in Hammam *et al*.[21] This was tested on the Honda Asimo platform. The acceleration of the non-contact limbs as a stabilization strategy has been used.[22] In that work, the 18-DOF robot is described using morphological data gathered from motion capture, and direct measurements of human subjects. The gait is controlled using a sliding mode control framework to increase robustness and to take into account modeling errors.

The use of the arms to assist stabilization and control has been considered. Park[23] has studied the implicit relationship of the arm swing and its effect on the ground reaction force of the stance foot. A more active role is given to both the trunk and the arms of the robot in stabilization against external forces in Zaoui *et al*.[24] In that work, a Proportional-Derivative (PD) controller takes information from a force/torque sensor, located between the waist and the trunk as the input for the controller. The use of the arms to interact with the environment in the event of disturbances is demonstrated.[25]

It is evident that the majority of the research in the dynamic stability of humanoid robots focuses on using the ZMP as the stabilization criteria. However, if a 3D model is used, the ZMP position *only represents at most three support reaction components*: one vertical force, one lateral moment component, and one longitudinal moment component. The lateral and longitudinal support forces and the vertical support moment are not represented by the ZMP position. These support force/moment components are also affected when a disturbance exists, or when the motion of a limb is modified in an effort to compensate for an existing disturbance. These support reaction forces and moments are normally provided by the limited frictional force/moment between the robot's foot and the ground. Foot sliding can occur if the lateral and longitudinal support force and the vertical support moment exceed the limit of the static friction force/moment between the robot's foot and the ground. Foot sliding can also lead to instabilities that can cause a fall. So, in some cases, controlling only the ZMP position is not sufficient to maintain the dynamic stability of the robot.

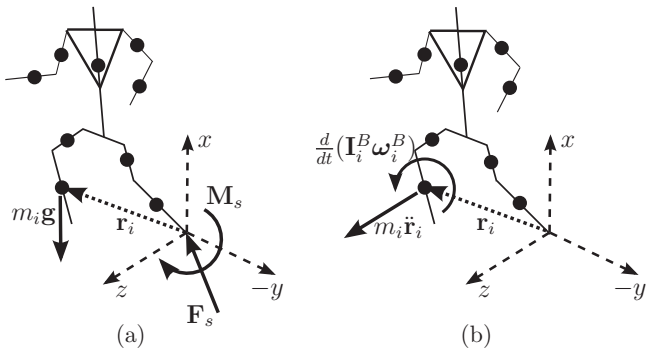

Fig. 1. (a) Free body diagram (FBD), (b) kinetic diagram (KD).

In this paper, all of the force and moment components of the support foot reaction are controlled, rather than just the position of the ZMP. By addressing all the support foot forces, not only is the tipping of the robot addressed but also the sliding of the support foot is prevented under bounded disturbances. Since up to a total of six components of the support reaction are controlled, up to 6 DOFs of the arms/body of the robot must be used for control. Here, the control inputs are the acceleration of joints, unlike more common approaches in which the positions of joints are used. In addition, an integral sliding mode controller is used in the control architecture to increase robustness of the controller. The outputs are taken from an integrated 6-DOF force/torque sensor that can be installed in the ankle of the robot's legs as discussed in Erbatur *et al*.[26]

2. Approach

In this paper, a method of control for the swing phase of a humanoid robot's walk is considered. The joint variables of the robot's limbs are denoted as $\mathbf{q}(t)$. Similarly, the desired joint trajectories that constitute a stable walking gait for the humanoid are denoted as $\mathbf{q}^d(t)$. A stable walking gait is one that does not cause the humanoid to tip over, or to enter into an irrecoverable state. A coordinate system is considered at the support foot. The x, y, and z-axes represent the vertical, lateral, and longitudinal directions respectively (Fig. 1a).

There are two conditions that must be met in order for the walking gait to be considered stable. The first condition states that the position of the ZMP must always be kept within the support polygon. The second condition states that the longitudinal and lateral forces (F_z, F_y), in addition to the vertical twist moment (M_x) of the support foot, cannot exceed the static friction limitation between the foot and the ground to prevent slipping. The ZMP equations are

$$\mathrm{ZMP}_z = \frac{M_y}{F_x}, \tag{1}$$

$$\mathrm{ZMP}_y = \frac{M_z}{F_x}. \tag{2}$$

The two conditions for a stable walk can be considered equivalent to maintaining a desired support force vector ($\mathbf{F}_R^d(t)$) and moment vector ($\mathbf{M}_R^d(t)$), where

$$\mathbf{F}_R = [F_x, F_y, F_z]^T, \mathbf{M}_R = [M_x, M_y, M_z]^T. \tag{3}$$

When these support reactions are controlled, the ZMP location as well as the support reactions provided by friction are controlled.

A desired value must be defined for the support reactions for control. The desired support force and moment vectors are those that exist in idealistic conditions, that is, when the robot is walking across perfectly level ground with no disturbances throughout the gait. They are calculated based on the joint trajectories of a stable walking gait.

https://doi.org/10.1017/S0263574714000332 Published online by Cambridge University Press

However, a humanoid robot that can walk only in idealistic conditions is not useful outside a perfect environment. Therefore, it is assumed that disturbances will exist during its walk, such as external forces/moments that act directly on the robot's body. These disturbances will affect the support force and moment vectors, causing them to deviate from their desired values.

In order to handle these disturbances, it is proposed to design a feedback controller to control the force and moment vectors in real-time to keep them at their desired values, regardless of the existence of disturbances. Specifically, an integral sliding mode architecture is chosen because of its robust nature in handling disturbances. The control output is defined as

$$\mathbf{y} = \begin{bmatrix} \mathbf{F}_R \\ \mathbf{M}_R \end{bmatrix}, \tag{4}$$

with the desired value

$$\mathbf{y}^d(t) = \begin{bmatrix} \mathbf{F}_R^d(t) \\ \mathbf{M}_R^d(t) \end{bmatrix}. \tag{5}$$

The following section focuses on the interaction of the forces and moments on the robot, and deriving the appropriate angular accelerations of the joints. The disturbance rejection control law is discussed in the next chapter. Finally, the simulation of the robot following the Conclusion ends the paper.

3. Input–Output Model

The input–output (I/O) model describes the interaction of the forces and moments on the robot. It serves as the basis on which the control is implemented. The equations are solved for the output variables in terms of the input variables. In the case of the robot, the reaction force and moment the robot's foot exerts on the ground, $\mathbf{F}_R$ and $\mathbf{M}_R$, are the output variables. The accelerations of the arm joints, $\ddot{\mathbf{q}}_a$, are the input variables. The force and moments are represented on the robot as a system of rigid bodies that are in a state of dynamic balance at time t. The free body diagram (FBD) and the kinetic diagram (KD) are shown in Fig. 1. $\mathbf{F}_s$ and $\mathbf{M}_s$ are the support force and moment the ground imparts to the robot's foot respectively. The variables m_i and $\mathbf{I}_i^B$ are the mass and centroidal moment of inertia matrices defined in local frame B for link i of the robot respectively. $\boldsymbol{\omega}_i^B$ is the angular velocity of link i in its local frame. $\mathbf{r}_i$ is the global position vector of the centroid of link i. $\mathbf{R}_{0i}$ is the rotation matrix that converts vector descriptions from the local frame of link i to the base inertial frame 0, specifically the base of the robot's left foot. It is important to note that $\mathbf{R}_{0i}$ is a function of $\theta_1, \theta_2, ..., \theta_i$. By equating the external forces and moments as shown in Fig. 1(a) with the inertial forces and moments shown in Fig. 1(b), Newton's second law, as applied to the robot shown, is

$$\mathbf{F}_s + \sum m_i \mathbf{g} = \sum m_i \ddot{\mathbf{r}}_i, \tag{6}$$

$$\mathbf{M}_s + \sum \mathbf{r}_i \times m_i \mathbf{g} = \sum (\mathbf{R}_{0i} \tfrac{d}{dt}(\mathbf{I}_i^B \boldsymbol{\omega}_i^B) + \mathbf{r}_i \times m_i \ddot{\mathbf{r}}_i). \tag{7}$$

The support force and moment are equal and opposite to the reaction force and moment, $\mathbf{F}_R$ and $\mathbf{M}_R$, that the robot exerts on the ground. That is, $\mathbf{F}_R = -\mathbf{F}_s$, and $\mathbf{M}_R = -\mathbf{M}_s$. From this, the reaction force and moment from the robot to the ground can replace the support force and moment in Eqs. (6) and (7). Isolating $\mathbf{F}_R$ and $\mathbf{M}_R$ gives

$$\mathbf{F}_R = \sum (m_i \mathbf{g} - m_i \ddot{\mathbf{r}}_i), \tag{8}$$

$$\mathbf{M}_R = \sum (\mathbf{r}_i \times m_i \mathbf{g} - \mathbf{R}_{0i}(\mathbf{I}_i^B \dot{\boldsymbol{\omega}}_i^B + \boldsymbol{\omega}_i^B \times \mathbf{I}_i^B \boldsymbol{\omega}_i^B) - \mathbf{r}_i \times m_i \ddot{\mathbf{r}}_i). \tag{9}$$

https://doi.org/10.1017/S0263574714000332 Published online by Cambridge University Press

The linear velocity of the center of mass of link i as expressed in the inertial frame ($\dot{\mathbf{r}}_i$) is derived in terms of the joint rate vector using Jacobian matrices,

$$\dot{\mathbf{r}}_i = \begin{bmatrix} \mathbf{J}_{ai} & \mathbf{J}_{bi} \end{bmatrix} \begin{bmatrix} \dot{\mathbf{q}}_a \\ \dot{\mathbf{q}}_b \end{bmatrix} \quad i = 1, ..., n. \tag{10}$$

Here, $\dot{\mathbf{q}}_a$ is a column vector containing the rates of the joints whose desired accelerations will be modified in real-time to control support reactions. The number of joints used is equal to the number of support reaction components that are going to be controlled. For a spatial robot, with six support reaction components, $\dot{\mathbf{q}}_a$ is 6×1. $\mathbf{J}_{ai}$ is the Jacobian matrix corresponding to $\dot{\mathbf{q}}_a$. For a spatial robot, this matrix is 3×6. This Jacobian matrix is defined as

$$\mathbf{J}_{ai} = \frac{\partial \dot{\mathbf{r}}_i}{\partial \dot{\mathbf{q}}_a^T} = \begin{bmatrix} \frac{\partial \dot{r}_{i1}}{\partial \dot{q}_{a1}} & \frac{\partial \dot{r}_{i1}}{\partial \dot{q}_{a2}} & \cdots & \frac{\partial \dot{r}_{i1}}{\partial \dot{q}_{aN}} \\ \frac{\partial \dot{r}_{i2}}{\partial \dot{q}_{a1}} & \frac{\partial \dot{r}_{i2}}{\partial \dot{q}_{a2}} & \cdots & \frac{\partial \dot{r}_{i2}}{\partial \dot{q}_{aN}} \\ \frac{\partial \dot{r}_{i3}}{\partial \dot{q}_{a1}} & \frac{\partial \dot{r}_{i3}}{\partial \dot{q}_{a2}} & \cdots & \frac{\partial \dot{r}_{i3}}{\partial \dot{q}_{aN}} \end{bmatrix}, \tag{11}$$

where N is the number of support forces to be controlled.

Here, $\dot{\mathbf{q}}_b$ is a column vector containing the joint rates of the remaining joints of the robot, whose desired trajectory remains unmodified during the motion. $\mathbf{J}_{bi}$ is the respective Jacobian matrix, and is defined in a similar manner as described for $\mathbf{J}_{ai}$. The relation for the angular velocity of the robot's links as expressed in the inertial frame $\boldsymbol{\omega}_i$ can be written as

$$\boldsymbol{\omega}_i = \begin{bmatrix} \mathbf{G}_{ai} & \mathbf{G}_{bi} \end{bmatrix} \begin{bmatrix} \dot{\mathbf{q}}_a \\ \dot{\mathbf{q}}_b \end{bmatrix} \quad i = 1, ..., n, \tag{12}$$

where $\mathbf{G}_{ai}$ and $\mathbf{G}_{bi}$ are of the same size as $\mathbf{J}_{ai}$ and $\mathbf{J}_{bi}$ respectively. These are also defined in a similar manner:

$$\mathbf{G}_{ai} = \frac{\partial \omega_i}{\partial \dot{\mathbf{q}}_a^T} = \begin{bmatrix} \frac{\partial \omega_{i1}}{\partial \dot{q}_{a1}} & \frac{\partial \omega_{i1}}{\partial \dot{q}_{a2}} & \cdots & \frac{\partial \omega_{i1}}{\partial \dot{q}_{aN}} \\ \frac{\partial \omega_{i2}}{\partial \dot{q}_{a1}} & \frac{\partial \omega_{i2}}{\partial \dot{q}_{a2}} & \cdots & \frac{\partial \omega_{i2}}{\partial \dot{q}_{aN}} \\ \frac{\partial \omega_{i3}}{\partial \dot{q}_{a1}} & \frac{\partial \omega_{i3}}{\partial \dot{q}_{a2}} & \cdots & \frac{\partial \omega_{i3}}{\partial \dot{q}_{aN}} \end{bmatrix}. \tag{13}$$

By taking the derivatives of the linear and angular velocities in Eqs. (10) and (12), the respective accelerations are found,

$$\begin{aligned} \ddot{\mathbf{r}}_i &= \mathbf{J}_{ai}\ddot{\mathbf{q}}_a + (\dot{\mathbf{J}}_{ai}\dot{\mathbf{q}}_a + \mathbf{J}_{bi}\ddot{\mathbf{q}}_b + \dot{\mathbf{J}}_{bi}\dot{\mathbf{q}}_b) \\ &= \mathbf{J}_{ai}\ddot{\mathbf{q}}_a + \mathbf{f}_{ti}, \end{aligned} \tag{14}$$

$$\begin{aligned} \dot{\boldsymbol{\omega}}_i &= \mathbf{G}_{ai}\ddot{\mathbf{q}}_a + (\dot{\mathbf{G}}_{ai}\dot{\mathbf{q}}_a + \mathbf{G}_{bi}\ddot{\mathbf{q}}_b + \dot{\mathbf{G}}_{bi}\dot{\mathbf{q}}_b) \\ &= \mathbf{G}_{ai}\ddot{\mathbf{q}}_a + \mathbf{f}_{ri}. \end{aligned} \tag{15}$$

https://doi.org/10.1017/S0263574714000332 Published online by Cambridge University Press

By substituting the accelerations into the force and moment equations from Eqs. (8) and (9), and rearranging the terms to isolate the joint accelerations $\ddot{\mathbf{q}}_a$, it can be shown

$$\begin{aligned}\mathbf{F}_R &= \left(-\sum m_i \mathbf{J}_{ai}\right)\ddot{\mathbf{q}}_a + \left(\sum m_i(\mathbf{g} - \mathbf{f}_{ti})\right) \\ &= \mathbf{b}_f \ddot{\mathbf{q}}_a + \mathbf{f}_f,\end{aligned} \tag{16}$$

$$\begin{aligned}\mathbf{M}_R = &\left[-\sum(\mathbf{R}_{0i}\mathbf{I}_i^B\mathbf{G}_{ai} + m_i\mathbf{r}_i \times \mathbf{J}_{ai})\right]\ddot{\mathbf{q}}_a \\ &+ \left[\sum(m_i\mathbf{r}_i \times \mathbf{g} - \mathbf{R}_{0i}(\boldsymbol{\omega}_i^B \times \mathbf{I}_i^B\boldsymbol{\omega}_i^B + \mathbf{I}_i^B\mathbf{f}_{ri}) - m_i\mathbf{r}_i \times \mathbf{f}_{ti}\right] \\ = &\ \mathbf{b}_m\ddot{\mathbf{q}}_a + \mathbf{f}_m.\end{aligned} \tag{17}$$

These force and moment equations can now be combined as a system of equations,

$$\begin{aligned}\begin{bmatrix}\mathbf{F}_R \\ \mathbf{M}_R\end{bmatrix} &= \begin{bmatrix}\mathbf{b}_f \\ \mathbf{b}_m\end{bmatrix}\ddot{\mathbf{q}}_a + \begin{bmatrix}\mathbf{f}_f \\ \mathbf{f}_m\end{bmatrix}, \\ \mathbf{y} &= \mathbf{b}\ddot{\mathbf{q}}_a + \mathbf{f}.\end{aligned} \tag{18}$$

The above model is valid when no disturbances act on the robot. Any external disturbance directly changes the support reactions, so an external disturbance can be viewed as a variation $\mathbf{d}_{\text{ext.}}$ in support reactions,

$$\mathbf{y} = \mathbf{b}\ddot{\mathbf{q}}_a + \mathbf{f} + \mathbf{d}_{\text{ext.}} \tag{19}$$

The desired reactions are derived by designing a stable gait for the robot in the absence of disturbances ($\mathbf{d}_{\text{ext.}} = \mathbf{0}$). The corresponding joint motions for the stable gait are described by $\mathbf{q}_a^d(t)$ and $\mathbf{q}_b^d(t)$. So the desired support reaction can be expressed as

$$\mathbf{y}^d = \mathbf{b}^d\ddot{\mathbf{q}}_a^d + \mathbf{f}^d, \tag{20}$$

where $\mathbf{b}^d$ and $\mathbf{f}^d$ are calculated using joint trajectories that cause a stable walk, that is, $\mathbf{q}_a^d(t)$ and $\mathbf{q}_b^d(t)$. At any given time, the difference between the current state of the robot with its desired state is

$$\mathbf{y} - \mathbf{y}^d = \mathbf{b}\ddot{\mathbf{q}}_a - \mathbf{b}^d\ddot{\mathbf{q}}_a^d + \mathbf{f} - \mathbf{f}^d + \mathbf{d}_{\text{ext.}} \tag{21}$$

The joint acceleration $\ddot{\mathbf{q}}_a$ is manipulated to compensate for the external disturbance. This causes the divergence of $\mathbf{q}_a$ from $\mathbf{q}_a^d(t)$. However, after the disturbance is eliminated, it is desirable that the joint positions $\mathbf{q}_a$ approach their originally planned trajectory for the stable walk. So, ideally, after the disturbance vanishes, the joint accelerations should be

$$\ddot{\mathbf{q}}_{a\,(\text{ideal})} = \ddot{\mathbf{q}}_a^d - (2\gamma\dot{\tilde{\mathbf{q}}}_a + \gamma^2\tilde{\mathbf{q}}_a), \tag{22}$$

where

$$\tilde{\mathbf{q}}_a = \mathbf{q}_a - \mathbf{q}_a^d, \tag{23}$$

and $\gamma > 0$. The form of Eq. (22) is selected such that the behavior of the error $\tilde{\mathbf{q}}_a = \mathbf{q}_a - \mathbf{q}_a^d$ is a critically damped second-order stable behavior. Choosing the coefficients of $\dot{\tilde{\mathbf{q}}}_a$ and $\tilde{\mathbf{q}}_a$ as 2γ and γ^2, respectively, generates that desired error behavior.

During the time that the disturbance is present, a different joint acceleration $\ddot{\mathbf{q}}_a$ is necessary. For the simplicity of the mathematical formulation, the difference between the ideal joint accelerations, Eq. (22), and the necessary joint accelerations during disturbance is selected as a control input,

$$\mathbf{u} = \ddot{\mathbf{q}}_a - \ddot{\mathbf{q}}_{a\,(\text{ideal}).} \tag{24}$$

https://doi.org/10.1017/S0263574714000332 Published online by Cambridge University Press

So the following policy is proposed for the way the acceleration of the arm is manipulated,

$$\ddot{\mathbf{q}}_a = \mathbf{u} + \ddot{\mathbf{q}}_a^d - (2\gamma\dot{\tilde{\mathbf{q}}}_a + \gamma^2\tilde{\mathbf{q}}_a). \tag{25}$$

The justification for this choice of system control input becomes more clear in Section 4.2, where the steady-state response of the control system is discussed.

Equation (25) is substituted in Eq. (21),

$$\mathbf{y} = \mathbf{bu} + (\mathbf{b} - \mathbf{b}^d)\ddot{\mathbf{q}}_a^d + \mathbf{f} - \mathbf{f}^d + \mathbf{y}^d - \mathbf{b}(2\gamma\dot{\tilde{\mathbf{q}}}_a + \gamma^2\tilde{\mathbf{q}}_a) + \mathbf{d}_{\text{ext.}}. \tag{26}$$

Equation (26) is rearranged,

$$\mathbf{y} = \mathbf{bu} + \mathbf{g} + \mathbf{d}_{\text{in.}} + \mathbf{d}_{\text{ext.}}, \tag{27}$$

where

$$\mathbf{g} = (\mathbf{b} - \mathbf{b}^d)\ddot{\mathbf{q}}_a^d + \mathbf{f} - \mathbf{f}^d + \mathbf{y}^d, \tag{28}$$

and

$$\mathbf{d}_{\text{in.}} = -\mathbf{b}(2\gamma\dot{\tilde{\mathbf{q}}}_a + \gamma^2\tilde{\mathbf{q}}_a). \tag{29}$$

Note that $\mathbf{d}_{\text{in.}}$ is not part of the dynamics of the real system. It is a disturbance on support reaction caused by trying to bring back the trajectories $\mathbf{q}_a$ onto $\mathbf{q}_a^d(t)$ after an external disturbance vanishes. The controller must be able to reject this "artificial" disturbance as well. Note that this disturbance is not know *a priori*, since the amount of deviation of the trajectories $\mathbf{q}_a$ from their desired value is a function of the amount and the duration of the external disturbance. However, the "artificial" disturbance is measurable in real-time.

Equation (27) constitutes the input–output model. In this model, the input is the deviation of the joint accelerations $\ddot{\mathbf{q}}_a$ from ideal joint accelerations $\ddot{\mathbf{q}}_{a(\text{ideal})}$, i.e., $\mathbf{u}$ in Eq. (25), and the output is the reaction force and moment, $\mathbf{F}_R$ and $\mathbf{M}_R$, collectively denoted by $\mathbf{y}$. Using this input–output model, one can design a controller to keep the support reaction components at their desired values. In the next section, the derivation of such a controller is presented.

4. Controller

In order for the humanoid robot to handle disturbances during its walking gait, it is crucial for the robot to implement a robust controller that can quickly and accurately carry out this duty. Without a controller, the robot could only perform in an ideal environment where it could execute its desired task without concern for any disturbances. In a real world environment, this is not useful, as a humanoid robot will need to compensate for external disturbances. Compensating for a disturbance consists of two parts: the robot must react to the disturbance, and then recover its motion by returning to the desired gait. In the following, first, a controller that can reject the disturbance is derived. Then the steady-state response of the system after the disturbance vanishes is investigated, and it is shown that the trajectories $\mathbf{q}_a$ asymptotically approach their desired values after the disturbance vanishes.

4.1. Control law derivations

For the robot in question, an algebraic input–output relation is determined between the input and output variables (Eq. 27) so that a control scheme can be utilized. The controller used in this paper is the integral sliding mode control. Any other robust control method can be used. For integral sliding

https://doi.org/10.1017/S0263574714000332 Published online by Cambridge University Press

mode control, a new state variable, $\mathbf{z}(t)$, is defined as the output variable,

$$\ddot{\mathbf{z}}(t) = \quad \mathbf{y}(t), \tag{30}$$

$$\dot{\mathbf{z}}(t) = \int_0^t \mathbf{y}(\tau)d\tau \quad \text{where } \dot{\mathbf{z}}(0) = \int_0^0 \mathbf{y}(\tau)d\tau = 0, \tag{31}$$

$$\mathbf{z}(t) = \int_0^t \dot{\mathbf{z}}(\tau)d\tau \quad \text{where } \mathbf{z}(0) = \int_0^0 \dot{\mathbf{z}}(\tau)d\tau = 0. \tag{32}$$

Output errors are defined as the difference between the measured and the desired value,

$$\tilde{\mathbf{z}} = \mathbf{z} - \mathbf{z}^d, \quad \dot{\tilde{\mathbf{z}}} = \dot{\mathbf{z}} - \dot{\mathbf{z}}^d, \quad \ddot{\tilde{\mathbf{z}}} = \ddot{\mathbf{z}} - \ddot{\mathbf{z}}^d, \tag{33}$$

where

$$\ddot{\mathbf{z}}^d(t) = \quad \mathbf{y}^d(t), \tag{34}$$

$$\dot{\mathbf{z}}^d(t) = \int_0^t \mathbf{y}^d(\tau)d\tau, \quad \text{where } \dot{\mathbf{z}}^d(0) = \int_0^0 \mathbf{y}^d(\tau)d\tau = 0, \tag{35}$$

$$\mathbf{z}^d(t) = \int_0^t \dot{\mathbf{z}}^d(\tau)d\tau, \quad \text{where } \mathbf{z}^d(0) = \int_0^0 \dot{\mathbf{z}}^d(\tau)d\tau = 0. \tag{36}$$

The nominal input–output model becomes

$$\ddot{\mathbf{z}} = \mathbf{b}\mathbf{u} + \mathbf{g}, \tag{37}$$

where $\mathbf{b}$ and $\mathbf{g}$ are defined in Eqs. (18) and (28). A first-order sliding surface is considered below,

$$\mathbf{s} = (\dot{\mathbf{z}} - \dot{\mathbf{z}}^d) + \mathbf{\Lambda}(\mathbf{z} - \mathbf{z}^d). \tag{38}$$

Note that, for integral sliding mode control, the states must start on the sliding surface at time zero, i.e., $\mathbf{s}(0)$ must be zero.[27,28] This condition is met with the way the new state variable, $\mathbf{z}(t)$, and its desired value, $\mathbf{z}^d(t)$, are defined in Eqs. (31), (32), (35), and (36).

The sliding surface is manipulated,

$$\begin{aligned} \mathbf{s} &= (\dot{\mathbf{z}} - \dot{\mathbf{z}}^d) + \mathbf{\Lambda}\tilde{\mathbf{z}}, \\ &= \dot{\mathbf{z}} - (\dot{\mathbf{z}}^d - \mathbf{\Lambda}\tilde{\mathbf{z}}), \\ &= \dot{\mathbf{z}} - \mathbf{s}_r, \end{aligned} \tag{39}$$

where $\mathbf{\Lambda}$ is a positive-definite diagonal square matrix. The following stable desired closed-loop system behavior is assumed,

$$\dot{\mathbf{s}} = \ddot{\mathbf{z}} - \dot{\mathbf{s}}_r = -\mathbf{K}\,\mathbf{sign}(\mathbf{s}), \tag{40}$$

where the gain, $\mathbf{K}$, is a diagonal positive definite matrix. The vector function $\mathbf{sign}(\mathbf{s})$ returns 1 or -1 for individual elements of $\mathbf{s}$ if the element is greater than zero or less than zero respectively. That is,

$$\mathbf{sign}(\mathbf{s}) = [\text{sign}(s_1), ..., \text{sign}(s_n)]^T.$$

This gain will cause $\mathbf{s}$ to vanish, and when $\mathbf{s}$ is zero, Eq. (39) guarantees that $\tilde{\mathbf{z}}$ and $\dot{\tilde{\mathbf{z}}}$ will tend to zero.

To derive the control law that generates the desired closed-loop system behavior (Eqs. 39 and 40), the nominal input–output model (Eq. 37) is substituted into Eq. (40). After solving for the input $\mathbf{u}$ it can be shown that

$$\mathbf{u} = \mathbf{b}^{-1}(-\mathbf{g} + \dot{\mathbf{s}}_r - \mathbf{K}\,\mathbf{sign}(\mathbf{s})). \tag{41}$$

https://doi.org/10.1017/S0263574714000332 Published online by Cambridge University Press

It must be shown that the control law (Eq. 41) can stabilize the actual system when a disturbance exists. It is assumed that the disturbance, $\mathbf{d} = \mathbf{d}_{\text{in.}} + \mathbf{d}_{\text{ext.}}$ exists. $\mathbf{d}_{\text{ext.}}$ is a bounded, unknown force/moment vector acting on the robot's body or limbs. The actual model of the system is

$$\ddot{\mathbf{z}} = \mathbf{bu} + \mathbf{g} + \mathbf{d}. \tag{42}$$

One of the goals of the integral sliding mode controller is to ensure that the sliding surface parameters will tend toward zero despite the existence of disturbances. A positive-definite Lyapunov function, V, is defined. That is,

$$V > 0. \tag{43}$$

Since a first-order stable sliding surface is considered (Eq. 39), the Lyapunov function must contain $\mathbf{s}$. A function using the norm of $\mathbf{s}$ is used,

$$V = \frac{1}{2}\|\mathbf{s}\|^2 = \frac{1}{2}\mathbf{s}^T\mathbf{s}. \tag{44}$$

As long as the time rate of the Lyapunov function is negative at all times, as defined in Eq. (43), $\mathbf{s}$ will vanish. Here, the condition on controller gain $\mathbf{K}$ is found to guarantee a negative rate for the Lyapunov function. The rate is calculated,

$$\dot{V} = \mathbf{s}^T\dot{\mathbf{s}}. \tag{45}$$

$\dot{\mathbf{s}}$ is replaced using Eq. (39):

$$\dot{V} = \mathbf{s}^T(\ddot{\mathbf{z}} - \dot{\mathbf{s}}_r). \tag{46}$$

Here, Eq. (42) is substituted for $\ddot{\mathbf{z}}$,

$$\dot{V} = \mathbf{s}^T(\mathbf{bu} + \mathbf{g} + \mathbf{d} - \dot{\mathbf{s}}_r). \tag{47}$$

Then $\mathbf{u}$ is replaced by Eq. (41),

$$\dot{V} = \mathbf{s}^T(\mathbf{bb}^{-1}(-\mathbf{g} + \dot{\mathbf{s}}_r - \mathbf{K}\,\mathbf{sign}(\mathbf{s})) + \mathbf{d} + \mathbf{g} - \dot{\mathbf{s}}_r). \tag{48}$$

After simplification, it is shown that

$$\begin{aligned}\dot{V} &= \mathbf{s}^T(-\mathbf{K}\,\mathbf{sign}(\mathbf{s}) + \mathbf{d}) \\ &= -\mathbf{s}^T\mathbf{K}\,\mathbf{sign}(\mathbf{s}) + \mathbf{s}^T\mathbf{d} \\ &= -\mathbf{s}^T\mathbf{K}\,\mathbf{sign}(\mathbf{s}) + \mathbf{d}^T\mathbf{s} \\ &= -\mathbf{s}^T\mathbf{K}\,\mathbf{sign}(\mathbf{s}) + \mathbf{d}_{\text{ext.}}^T\mathbf{s} + \mathbf{d}_{\text{in.}}^T\mathbf{s}.\end{aligned} \tag{49}$$

A bound is assumed for the elements of the disturbance vector,

$$|d_{i\ \text{ext.}}| \leq D_{i\ \text{ext.}}. \tag{50}$$

Note that, normally, the bound ($D_{i\ \text{ext.}}$) is found by trial and error via simulations. A high value is selected, and disturbances close to the chosen bound are applied to the robot in simulation. If the required control action to reject the disturbance is not affordable by the robot, the selected upper limit is too high and needs to be reduced.

https://doi.org/10.1017/S0263574714000332 Published online by Cambridge University Press

The terms in Eq. (49) are manipulated as explained in Appendix. After the manipulation, Eq. (49) becomes

$$\begin{aligned}\dot{V} &\leq -\mathbf{K}_v\,|\mathbf{s}| + \mathbf{D}^T_{\text{ext.}}|\mathbf{s}| + |\mathbf{d}^T_{\text{in.}}||\mathbf{s}|,\\ &\leq -(\mathbf{K}_v - \mathbf{D}^T_{\text{ext.}} - |\mathbf{d}^T_{\text{in.}}|)|\mathbf{s}|.\end{aligned} \tag{51}$$

where $\mathbf{K}_v = [K_{11}, \ldots, K_{nn}]$ is a row vector containing the diagonal elements of the diagonal matrix $\mathbf{K}$, and $|\mathbf{s}| = [|s_1|, \ldots, |s_n|]^T$.

Equation (51) implies that if the elements of $\mathbf{K}_v$ are selected such that they are larger than the corresponding elements of $\mathbf{D}^T_{\text{ext.}} + |\mathbf{d}^T_{\text{in.}}|$, then the rate of the Lyapunov function is negative, and $\mathbf{s}$ vanishes despite the existence of any bounded external disturbance that satisfies Eq. (50). In the form of an equation,

$$\mathbf{K}_v \geq \mathbf{D}^T_{\text{ext.}} + |\mathbf{d}^T_{\text{in.}}| + \boldsymbol{\eta}^T, \tag{52}$$

where $\boldsymbol{\eta}$ is a column vector with positive elements.

It is important to note that in practical situations, sliding mode control signal chattering must be eliminated by replacing the sign function (**sign**(**s**)) in Eq. (41) with a saturation function. For example,

$$\mathbf{sat}(\mathbf{s}) = [\text{sat}(s_1), ..., \text{sat}(s_n)]^T,$$

where

$$\text{sat}(s_i) = \begin{cases} \text{sign}(s_i) & \text{if } |s_i| \geq \phi \\ s_i/\phi & \text{if } |s_i| < \phi \end{cases},$$

in which $\phi > 0$ is known as the sliding surface boundary layer.

4.2. Steady-state response after the external disturbance vanishes

When a disturbance is present, the controller modifies the trajectory of the joints $\mathbf{q}_a$ to reject the disturbance. This causes the deviation of the trajectory of joints $\mathbf{q}_a$ from the desired trajectory such that the output (i.e. the force and moment reactions under the support foot) remain equal to the desired output. After the disturbance is eliminated, it is desirable that the joints $\mathbf{q}_a$ approach their originally planned trajectories. The choice of the control input (Eq. 25) guarantees asymptotic convergence of the joint trajectories $\mathbf{q}_a$ to their planned trajectory. In the following, the steady-state response of the system in absence of the disturbance is derived, which shows a stable trajectory for $\mathbf{q}_a$.

The response of the actual plant is represented by Eq. (19), which is repeated here for convenience,

$$\mathbf{y} = \mathbf{b}\ddot{\mathbf{q}}_a + \mathbf{f} + \mathbf{d}_{\text{ext.}} \tag{53}$$

It is assumed that the external disturbance vanishes at some time, that is, $\mathbf{d}_{\text{ext.}} = \mathbf{0}$. At the steady-state, the output $\mathbf{y}$ has already converged to its desired value, so

$$\mathbf{y} = \mathbf{y}^d \Rightarrow \mathbf{s} = \mathbf{0}, \quad \dot{\mathbf{s}}_r = \ddot{\mathbf{z}}^d = \mathbf{y}^d. \tag{54}$$

These conditions are substituted in the control law (Eq. 41). The control input at the steady-state becomes

$$\mathbf{u}_{ss} = \mathbf{b}^{-1}(-(\mathbf{b} - \mathbf{b}^d)\ddot{\mathbf{q}}^d_a - \mathbf{f} + \mathbf{f}^d - \mathbf{y}^d + \mathbf{y}^d). \tag{55}$$

The arm joint accelerations at steady-state are determined by Eq. (25),

$$\ddot{\mathbf{q}}_{a(ss)} = \mathbf{u}_{ss} + \ddot{\mathbf{q}}^d_a - (2\gamma\dot{\tilde{\mathbf{q}}}_a + \gamma^2\tilde{\mathbf{q}}_a). \tag{56}$$

https://doi.org/10.1017/S0263574714000332 Published online by Cambridge University Press

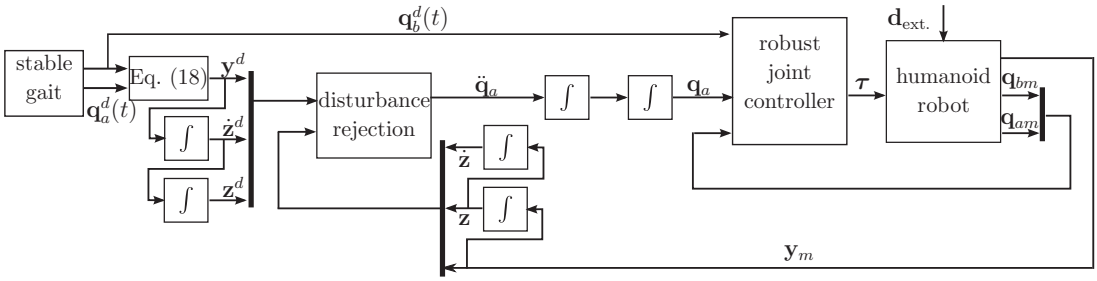

Fig. 2. Block diagram.

Equations (55) and (56), in addition to Eq. (20), are substituted in Eq. (19), with $\mathbf{d}_{\text{ext.}} = \mathbf{0}$ and $\mathbf{y} = \mathbf{y}^d$. The result is

$$\mathbf{b}(2\gamma\dot{\tilde{\mathbf{q}}}_a + \gamma^2\tilde{\mathbf{q}}_a) = \mathbf{0}. \tag{57}$$

It must be noted that $\mathbf{b}$ is, in fact, the robot's mass matrix, i.e., the multiplier of the joint accelerations $\ddot{\mathbf{q}}_a$, in its equations of motion (Eqs. 16–18). The mass matrix is positive definite for all values of $\mathbf{q}_a$ as long as singularities are avoided. So Eq. (57) is rewritten as

$$\dot{\tilde{\mathbf{q}}}_a + \left(\frac{\gamma}{2}\right)\tilde{\mathbf{q}}_a = \mathbf{0}. \tag{58}$$

Since $\gamma > 0$, Eq. (58) indicates that the arm trajectories will asymptotically approach their desired value at the steady-state when the external disturbance vanishes.

4.3. Controller block diagram

The entire control scheme consists of three subsystems: desired output, disturbance rejection, and the robust joint control. These are shown together in Fig. 2.

In the subsystem that generates the desired outputs $\mathbf{y}^d$ (the support force and moment components), the nominal trajectories are defined for the joints of the robot, $\mathbf{q}_a^d(t)$ and $\mathbf{q}_b^d(t)$. These trajectories are designed in such a way that the requirements of a stable walk are met, as described in Section 2. To reiterate, these requirements are confining the ZMP within the support polygon during the walking cycle, and keeping the longitudinal and lateral support forces and the support twist moment lower than the maximum static friction between the support foot and the ground. With these requirements met, $\mathbf{y}^d$ yields a desirable, stable walking gait.

The subsystem that modifies the trajectory of robot's joints $\mathbf{q}_a$ to maintain the desired output ($\mathbf{y}^d$) contains the disturbance rejection controller. This subsystem receives the desired output and its associated integrals, as well as the measured output, $\mathbf{y}_m$. The measured output is provided by a 6-DOF force/torque sensor installed in the robot's ankle, similar to that of Erbatur *et al.*,[26] where a 6-DOF force/torque sensor transmits force and moment data. The output of the disturbance rejection control system is the modified joint motion for $\mathbf{q}_a$, which is found in real-time by integrating Eq. (25).

Lastly, the subsystem that controls the motion of the robot's joints is considered. This subsystem receives the desired motion of the body and legs ($\mathbf{q}_b^d(t)$), and the modified arm motion ($\mathbf{q}_a$). The torques of the joints (τ) are calculated from the measured joint positions ($\mathbf{q}_{am}$, $\mathbf{q}_{bm}$) by a robust joint controller, however this particular controller is beyond the focus of this paper and has no bearing on the outcome of the simulations. A user of the proposed method can freely use their own existing joint controller, or derive their own joint controller using their favorite control method. This controller must be able to perfectly perform the desired joint motion despite the existence of potential bounded disturbances. Low-level sliding mode robust controllers can easily meet this requirement.[29,30]

https://doi.org/10.1017/S0263574714000332 Published online by Cambridge University Press

Fig. 3. The 18-DOF humanoid robot whose model is used for simulations.

Table I. Link parameters for the 18-DOF humanoid.

Joint i	a_{i-1}	α_{i-1}	θ_i	Mass	P_X	P_Y	P_Z
	(mm)	(deg)	(deg)	(gm)	(mm)	(mm)	(mm)
1 (R ankle)	0.0	0	q_1	125	12.7	0.4	−16.0
2 (R ankle)	0.0	−90	q_2	76	65.0	−11.4	0.6
3 (R knee)	77.5	0	q_3	22	33.2	−7.2	0.0
4 (R hip)	78.0	0	q_4	125	−12.7	16.1	0.4
5 (R hip)	0.0	90	$q_5 - 90$	11	0.0	19.0	−16.5
6 (R hip)	0.0	−90	$q_6 + 180$	321	39.4	−11.4	84.7
7 (L hip)	77.0	0	q_7	11	0.0	−16.5	19.0
8 (L hip)	0.0	−90	$q_8 - 90$	125	−12.7	0.36	16.0
9 (L hip)	0.0	−90	$q_9 - 180$	22	43.2	7.3	0.0
10 (L knee)	78.0	0	q_{10}	76	11.4	11.3	−0.6
11 (L ankle)	77.5	0	$q_{11} + 180$	125	−12.7	−16.0	0.4
12 (L ankle)	0.0	90	q_{12}	32	25.8	0.0	4.8
13 (R shoulder)	0.0	0	q_{13}	9	3.8	0.0	−12.2
14 (R shoulder)	14.5	90	q_{14}	69	18.6	0.0	0.7
15 (R elbow)	67.5	0	q_{15}	74	22.4	0.9	0.6
16 (L shoulder)	0.0	0	q_{16}	9	3.8	0.0	−12.2
17 (L shoulder)	14.5	−90	q_{17}	69	18.5	0.0	0.7
18 (L elbow)	67.5	0	q_{18}	74	22.4	−0.8	0.6

5. Simulation

As an example, a spatial 18-DOF biped robot is considered (Fig. 3). The joints are shown by circular markers. The degrees of freedom of the robot, its Denavit–Hartenberg parameters, and its link mass information are listed in Table I.

Here, the left arm (q_{13}, q_{14}, q_{15}) and the right arm (q_{16}, q_{17}, q_{18}) are used for manipulating the vertical, lateral, and longitudinal support forces (F_x, F_y, F_z) and moments (M_x, M_y, M_z). So $\mathbf{q}_a = [q_{13}, q_{14}, q_{15}, q_{16}, q_{17}, q_{18}]^T$ and $\mathbf{y} = [F_x, F_y, F_z, M_x, M_y, M_z]^T$. The Denavit–Hartenberg parameters and the mass distribution information in Table I are used to derive the Jacobian matrices in Eqs. (11) and (13). The Jacobian matrices are then substituted in Eqs. (16) and (17) to give the general form (18). This general form simulates a real 18-DOF robot, and is used to calculate the support forces $\mathbf{y}$ that a real 18-DOF robot would experience under disturbances in real-time.

Any gait planning method can be used to plan a stable gait for the robot.[31,32] Here, for simplicity, 7º polynomials in time are used to plan the trajectory of the joints from start to the end of the step. Jerk, acceleration, and speed of the joints are zero at both the start and the end of the step. The joint

https://doi.org/10.1017/S0263574714000332 Published online by Cambridge University Press

Table II. Robot's joint angles at the start and end of a step in degrees.

	q_1	q_2	q_3	q_4	q_5	q_6	q_7	q_8	q_9
Start	0	0	−24	24	0	0	0	0	18
End	0	17	−17	0	0	0	0	−25	
	q_{10}	q_{11}	q_{12}	q_{13}	q_{14}	q_{15}	q_{16}	q_{17}	q_{18}
Start	0	73	0	0	0	0	0	0	0
End	−336	73	0	0	0	0	0	0	0

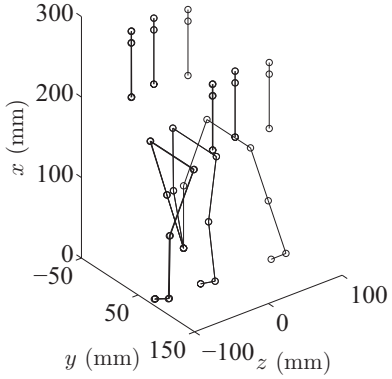

Fig. 4. Schematic view of the 3D 18-DOF biped robot's gait. The joints are shown by circular markers.

angles at the beginning and the end of the step are listed in Table II. One step takes 1.0 s and is 90-cm long. Snapshots of motion are shown in Fig. 4.

The controller modifies the acceleration of q_{13}, q_{14}, q_{15}, q_{16}, q_{17}, q_{18} to control the support forces at the desired level equivalent to the case where no disturbance is present. That is, the motion of the arms and body are modified by the controller in real-time such that the support force/moment components are not affected.

The controller gains are as follows:

$$\begin{gathered}\gamma = 10,\\ \mathbf{\Lambda} = \begin{bmatrix}1 & 0 & 0\\ 0 & 1 & 0\\ 0 & 0 & 1\end{bmatrix},\\ \mathbf{D}_{\text{ext.}}^T = \begin{bmatrix}2.7 & 2.7 & 2.7 & 0.41 & 0.41 & 0.41\end{bmatrix},\\ \boldsymbol{\eta}^T = \begin{bmatrix}1 & 1 & 1 & 1 & 1 & 1\end{bmatrix},\\ \phi = 0.01,\end{gathered} \tag{59}$$

where the units of the elements of $\mathbf{D}_{\text{ext.}}$ are Newton, Newton, Newton, Newton-meter, Newton-meter, and Newton-meter, respectively.

In this example, the ZMP location and the support forces corresponding to the defined desired trajectory are desirable. The feet of the robot are large enough to cover the variation of the ZMP position for the whole desired walking cycle of this robot. First, the desired joint trajectories are used to calculate the desired vertical, lateral, and longitudinal force (F_x^d, F_y^d, F_z^d) and moment (M_x^d, M_y^d, M_z^d) that the robot exerts on the ground during a step. These forces and moments are valid when the robot walks in the absence of any external disturbances. Here, these values are referred to as "desired" values.

A disturbance is assumed to act on the robot from time 0.45 s to 0.55 s, in the middle of the 1.0-s step. The disturbance is a smooth varying horizontal force, with two equal y (lateral) and z (longitudinal) components. Each component has a peak of 2.7 N (20% of the robot's weight) on the

https://doi.org/10.1017/S0263574714000332 Published online by Cambridge University Press

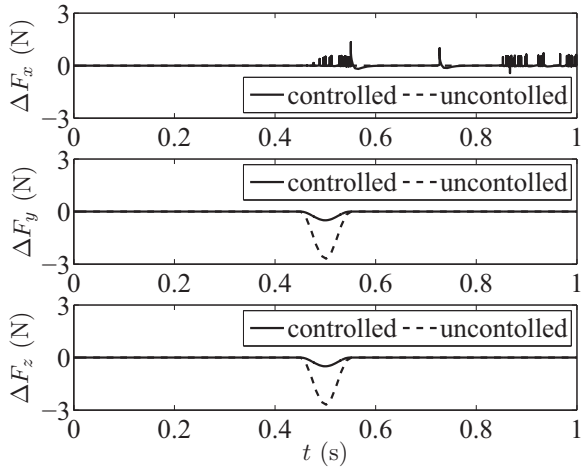

Fig. 5. The effect of the disturbance on the support reaction. $\Delta F_x = F_x - F_z^d$, $\Delta F_y = F_y - F_y^d$, and $\Delta F_z = F_z - F_z^d$. Controlled (solid curve): change in support reaction with disturbance when the proposed controller is used. Uncontrolled (dashed curve): change in support reaction with disturbance when no controller is used.

robot's body at a height of 0.15 m. This force also generates moment about the foot that is on the ground. So the disturbance vector has the following form,

$$\mathbf{d}_{\text{ext.}} = \begin{bmatrix} 0 \\ -2.7\left(1-\cos\left(\frac{2\pi(t-0.45)}{0.1}\right)\right)/2 \\ -2.7\left(1-\cos\left(\frac{2\pi(t-0.45)}{0.1}\right)\right)/2 \\ 0 \\ 2.7(0.15)\left(1-\cos\left(\frac{2\pi(t-0.45)}{0.1}\right)\right)/2 \\ 2.7(0.15)\left(1-\cos\left(\frac{2\pi(t-0.45)}{0.1}\right)\right)/2 \end{bmatrix} \quad 0.45 \le t \le 0.55. \tag{60}$$

Note that the controller plans joint accelerations to reject the disturbance. Under constant-active disturbances, the controller keeps accelerating the joints, which may cause the joints to move close to their physical limits. So, practically, constant-active disturbances cannot be supported. That is why a part-time disturbance is used.

Figure 5 shows the change in the support force due to the application of the disturbance for the cases where the controller is used (solid curves), and where the controller is not used (dashed curves). It can be seen that for both the cases, the changes in the vertical component (F_x) is negligible, because the disturbance force does not act in this direction. The change in the longitudinal and lateral force components is significant when the controller is not used, whereas that change is negligible with the use of the controller.

Figure 6 shows the change in the support moment due to the application of the disturbance for the cases where the controller is used (solid curves), and where the controller is not used (dashed curves). It can be seen that for both the cases, the changes in the vertical component (F_x) is negligible, because the disturbance moment does not act in that direction. The change in the lateral and longitudinal moment components is significant when the controller is not used, whereas that change is negligible with the use of the controller.

The longitudinal and the lateral shifts in the ZMP position is compared in Fig. 7. The longitudinal and lateral positions of the ZMP are calculated by dividing M_y by F_x, and by dividing M_z by F_x. Shifts in the longitudinal and lateral ZMP positions are calculated by subtracting the longitudinal and

https://doi.org/10.1017/S0263574714000332 Published online by Cambridge University Press

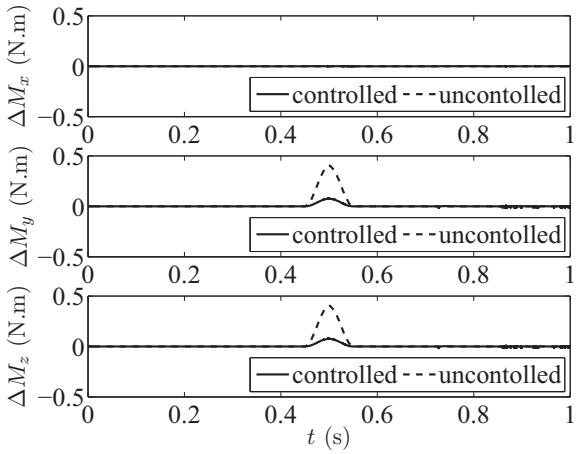

Fig. 6. The effect of the disturbance on the support reaction. $\Delta M_x = M_x - M_z^d$, $\Delta M_y = M_y - M_y^d$, and $\Delta M_z = M_z - M_z^d$. Controlled (solid curve): change in support reaction with disturbance when the proposed controller is used. Uncontrolled (dashed curve): change in support reaction with disturbance when no controller is used.

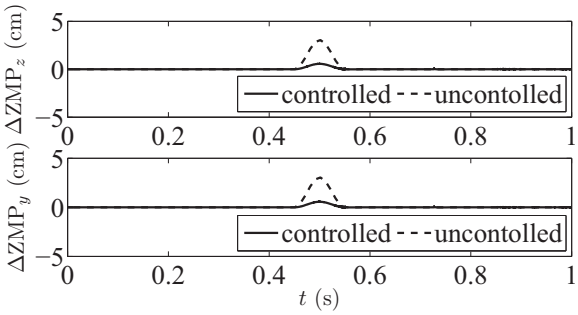

Fig. 7. Longitudinal and lateral ZMP shifts. Uncontrolled (dashed curves): ZMP shift with disturbance when no controller is used. Controlled (solid curves): ZMP shift with disturbance when the proposed controller is used.

lateral ZMP positions of the disturbed (uncontrolled and controlled) cases with that of the "desired" case (where there is no disturbance). The curves labeled as "uncontrolled" represent how the ZMP shifts when no controller is used.

It can be seen that the longitudinal and lateral ZMP positions have shifted more than 3 cm due to the large disturbance. This can easily cause the robot to lose its balance during the walk if the desired longitudinal ZMP is closer than 3 cm to the edge of the foot. For example, if the size of the sole is 5 cm and the longitudinal ZMP is originally at the center of the foot (2.5 cm from the edge of the foot), the robot will loose its balance with the applied disturbance. The curves labeled as "controlled" represent how the ZMP positions shift when the proposed controller is used. The shift of the longitudinal ZMP position is less than 1 cm when the disturbance rejection controller is used. This means that if the original gait planned for the robot has a stable ZMP position, that ZMP position will be held very closely by the disturbance rejection controller despite the presence of a disturbance. So the robot's walk will remain stable even when the disturbance is present. Simulations showed that using very high controller gains eliminates the small shift shown in Fig. 7 for the controlled case. However, moderate gains have been used to depict a more realistic scenario, which prevents chatter in the control input.

Figure 8 shows the change in the required coefficient of static friction to prevent slip. The required coefficient of friction to prevent slip in the lateral and longitudinal directions are $\mu_y = \frac{F_y}{F_x}$ and $\mu_z = \frac{F_z}{F_x}$ respectively. These values are different when the controller is on or off. The difference of these coefficients of static friction are plotted in Fig. 8. The second plot in this figure indicates that the required coefficient of static friction to prevent slip is approximately 0.25 smaller when the controller

https://doi.org/10.1017/S0263574714000332 Published online by Cambridge University Press

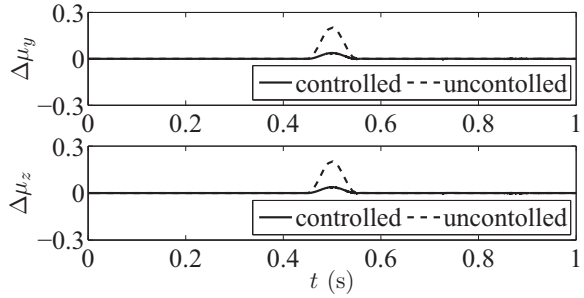

Fig. 8. Change in the required coefficient of static friction to prevent slip. Uncontrolled: disturbance is present while the controller is off. Controlled: disturbance is present while the controller is on.

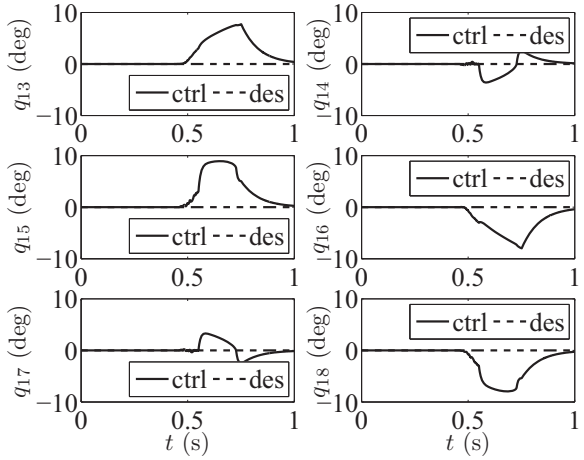

Fig. 9. The trajectory of the arms. (des = desired): desired trajectories of the arms. (ctrl = controlled): trajectories of the arms with disturbance when the proposed controller is used.

is used. This means that the robot is less likely to slip in the longitudinal and lateral directions when the controller is on.

The modified trajectory of the arms and the body are compared with the original ones in Fig. 9. A slight motion of the arms has been used by the controller to reject the disturbance. After the disturbance is eliminated, the arms return to their desired trajectory.

6. Conclusions

A disturbance rejection controller is proposed in general form based on the 3D dynamics of biped robots, and applied to an 18-DOF biped humanoid robot. The swing phase of the robot's walking gait is considered. An integral sliding mode architecture is chosen for the disturbance rejection, where the support forces and moments of the support foot are chosen as the outputs and the acceleration of the arm/body joints is chosen as the inputs. It is assumed that the support reactions are gathered from force sensors mounted on a "shoe" on the bottom of the robot's feet. The position, velocity, and acceleration of the joints are gathered from the servo motors of the robot.

During the disturbance rejection, the arm/body joints deviate slightly from their desired trajectory, while the leg joints remain at their desired trajectory. This has important implications during tasks where foot placement or specific leg positions are critical, i.e., the stepping stone problem. Since the leg joint trajectories are unaffected, the robot will still be able to complete the task, even when bounded disturbances are experienced. The controller utilizes the full dynamic model of the robot. This provides an accurate representation of the robot's gait and its reactions to forces.

The proposed controller can successfully mitigate bounded disturbances to maintain the desired value of all support reactions. Even the support reactions that are not represented by the ZMP position, i.e., the longitudinal and lateral support forces and the vertical twist moment, are unchanged during

https://doi.org/10.1017/S0263574714000332 Published online by Cambridge University Press

the application of the disturbance. This ensures that the robot's foot does not slip under disturbance, a feature that is lacking on other disturbance rejection approaches.

In addition, the controller can eliminate the shift in the position of the ZMP. By eliminating the shift in the ZMP position, the robot does not tip under the disturbance. This paper shows that using a sliding mode architecture to reject bounded disturbances by only modifying the accelerations of the selected joints is a successful approach to biped humanoid stable walking.

References

1. T. McGeer, "Passive dynamic walking," *Int. J. Robot. Res.* **9**(2), 62–82 (1990).
2. Z. Liu, A. Zhang, Y. Tian, P. Zhang and D. Gao, "Further Analysis of the Kneed Passive-Dynamic Biped Robot," *Proceedings of Chinese Control and Decision Conference (CCDC 2010)*, Xuzhou, China (2010) pp. 1777–1782.
3. K. Hitomi, T. Shibata, Y. Nakamura and S. Ishii, "Reinforcement learning for quasi-passive dynamic walking of an unstable biped robot," *Robot. Auton. Syst.* **54**(12), 982–988 (2006).
4. M. Vukobratovic and B. Borovac, "Zero moment point – thirty five years of its life," *Int. J. Humanoid Robot* **1**(1), 157–173 (2004).
5. R. Zhang, P. Vadakkepat and C. M. Chew, "Motion Planning for Biped Robot Climbing Stairs," *Proceedings of FIRA Robot World Congress*, Vienna, Austria (Oct. 1–3, 2003) pp. 1–6.
6. K. Hirai, Y. H. M. Hirose and T. Takenaka, "The Development of Honda Humanoid Robot," *Proceedings of the IEEE International Conference on Robotics and Automation*, vol. 2 (1998) pp. 1321–1326.
7. V. Prahlad, G. Dip and C. Meng-Hwee, "Disturbance rejection by online ZMP compensation," *Robotica* **26**, 9–17 (2008).
8. N. Naksuk, C. S. G. Lee and S. Rietdyk, "Whole-Body Human-to-Humanoid Motion Transfer," *Proceedings of the 5th IEEE-RAS International Conference on Humanoid Robots*, Tsukuba, Japan, vol. 2005 (2005) pp. 104–109.
9. A. Sano and J. Furusho, "Realization of Natural Dynamic Walking Using the Angular Momentum Information," *Proceedings of the IEEE International Conference on Robotics and Automation*, vol. 3 (May 1990) pp. 1476 –1481.
10. Y. Okumura, T. Tawara, K. Endo, T. Furuta and M. Shimizu, "Real-Time ZMP Compensation for Biped Walking Robot Using Adaptive Inertia Force Control," *Proceedings of IEEE/RSJ International Conference on Intelligent Robots and Systems (IROS 2003)*, Piscataway, NJ, vol. 1 (2003) pp. 335–339.
11. I.-W. Park, J.-Y. Kim and J.-H. Oh, "Online walking pattern generation and its application to a biped humanoid robot – KHR-3 (HUBO)," *Adv. Robot.* **22**(2–3), 159–190 (2008).
12. H. O. Lim, Y. Kaneshima and A. Takanishi, "Online Walking Pattern Generation for Biped Humanoid Robot with Trunk," *Proceedings of IEEE International Conference on Robotics and Automation*, vol. 3 (2002) pp. 3111–3116.
13. J. Yamaguchi, E. Soga, S. A. Setiawan, D. Aoyagi, A. Nagamatsu and A. Takanishi, "Development of a bipedal humanoid robot presupposing various whole body motions," *Adv. Robot.* **13**(3), 297–299 (1999).
14. K. Mitobe, G. Capi and Y. Nasu, "Control of walking robots based on manipulation of the zero moment point," *Robotica* **18**(6), 651–657 (2000).
15. J. Vermeulen, B. Verrelst, D. Lefeber, P. Kool and B. Vanderborght, "A real-time joint trajectory planner for dynamic walking bipeds in the sagittal plane," *Robotica* **23**(6), 669–680 (2005).
16. J. H. Park and H. Chung, "ZMP Compensation by Online Trajectory Generation for Biped Robots," *Proceedings of IEEE International Conference on Robotics and Automation*, vol. 4 (Oct. 10–15, 1999) pp. 960–965.
17. T. Sugihara, Y. Nakamura and H. Inoue, "Realtime Humanoid Motion Generation Through ZMP Manipulation Based on Inverted Pendulum Control," *Proceedings of the IEEE International Conference on Robotics and Automation*, Washington, DC, vol. 2 (2002) pp. 1404–1409.
18. K. Erbatur and O. Kurt, "Humanoid Walking Robot Control with Natural ZMP References," *Proceedings of the Industrial Electronics Conference (IECON)*, Paris, France (2006) pp. 4100–4106.
19. S. Kajita, F. Kanehiro, K. Kaneko, K. Yokoi and H. Hirukawa, "The 3D Linear Inverted Pendulum Mode: A Simple Modeling for a Biped Walking Pattern Generation," *Proceedings of the IEEE International Conference on Intelligent Robots and Systems*, Maui, HI, vol. 1 (2001) pp. 239–240.
20. B.-J. Lee, D. Stonier, Y.-D. Kim, J.-K. Yoo and J.-H. Kim, "Modifiable Walking Pattern Generation Using Real-Time ZMP Manipulation for Humanoid Robots," *Proceedings of the IEEE International Conference on Intelligent Robots and Systems*, San Diego, CA (2007) pp. 4221–4226.
21. G. B. Hammam, D. Orin and B. Dariush, "Whole-Body Humanoid Control from Upper-Body Task Specifications," *Proceedings of IEEE International Conference on Robotics and Automation (ICRA)* (May 3–7, 2010) pp. 3398–3405.
22. A. Hofmann, S. Massaquoi, M. Popovic and H. Herr, "A Sliding Controller for Bipedal Balancing Using Integrated Movement of Contact and Non-Contact Limbs," *Proceedings of IEEE/RSJ International Conference on Intelligent Robots and Systems (IROS)*, Sendai, Japan, vol. 2 (2004) pp. 1952–1959.
23. J. Park, "Synthesis of natural arm swing motion in human bipedal walking," *J. Biomech.* **41**(7), 1417–1426 (2008).

https://doi.org/10.1017/S0263574714000332 Published online by Cambridge University Press

24. C. Zaoui, O. Bruneau, F. Ouezdou and A. Maalej, "Simulations of the dynamic behavior of a bipedal robot with trunk and arms subjected to 3D external disturbances in a vertical posture, during walking and during object handling," *Multibody Syst. Dyn.* **21**(3), 261–280 (2009).
25. C.-B. Yin, Q.-M. Zhou, H.-H. Xu and M. Yang, "Stability maintenance of a humanoid robot under external disturbance," *Kongzhi yu Juece* (*Control Decis.*) **21**(6), 619–624 (2006).
26. K. Erbatur, U. Seven, E. Taskiran, O. Koca, M. Yilmaz, M. Unel, G. Kiziltas, A. Sabanovic and A. Onat, "SURALP: A New Full-Body Humanoid Robot Platform," *2009 IEEE/RSJ International Conference on Intelligent Robots and Systems (IROS 2009)*, St. Louis, MO (2009) pp. 4949–4954.
27. W.-J. Cao and J.-X. Xu, "Nonlinear integral-type sliding surface for both matched and unmatched uncertain systems," *IEEE Trans. Autom. Control* **49**(8), 1355–1360 (2004).
28. F. Castanos and L. Fridman, "Analysis and design of integral sliding manifolds for systems with unmatched perturbations," *IEEE Trans. Autom. Control* **51**(5), 853–858 (2006).
29. J.-J. E. Slotine and W. Li, *Applied Nonlinear Control* (Prentice-Hall, Upper Saddle River, NJ, 1991), Ch. 9, pp. 397–402.
30. M. Nikkhah, H. Ashrafiuon and F. Fahimi, "Robust control of underactuated bipeds using sliding modes," *Robotica* **25**(3), 367–374 (2007).
31. S. A. A. Moosavian, M. Alghooneh and A. Takhmar, "Cartesian approach for gait planning and control of biped robots on irregular surfaces," *Int. J. Humanoid Robot.* **6**(4), 675–697 (2009).
32. K.-Y. Tu and M.-S. Liu, "Planning of sagittal gait of biped robots based on minimum motion energy," *Int. J. Humanoid Robot.* **7**(4), 635–667 (2010).

Appendix

In Eq. (49), the following has been used.

$$\begin{aligned}
\mathbf{s}^T\mathbf{K}\,\mathbf{sign}(\mathbf{s}) &= \begin{bmatrix} s_1 & \dots & s_n \end{bmatrix} \begin{bmatrix} K_{11} & \dots & 0 \\ \vdots & \vdots & \vdots \\ 0 & \dots & K_{nn} \end{bmatrix} \begin{bmatrix} \text{sign}(s_1) \\ \vdots \\ \text{sign}(s_n) \end{bmatrix}, \\
&= \begin{bmatrix} s_1 & \dots & s_n \end{bmatrix} \begin{bmatrix} K_{11}\ \text{sign}(s_1) \\ \vdots \\ K_{nn}\ \text{sign}(s_n) \end{bmatrix}, \\
&= s_1 K_{11}\ \text{sign}(s_1) + \cdots + s_n K_{nn}\ \text{sign}(s_n), \\
&= K_{11}|s_1| + \cdots + K_{nn}|s_n|, \\
&= \begin{bmatrix} K_{11} & \dots & K_{nn} \end{bmatrix} \begin{bmatrix} |s_1| \\ \vdots \\ |s_n| \end{bmatrix}, \\
&= \mathbf{K}_v|\mathbf{s}|.
\end{aligned}$$

Also,

$$\begin{aligned}
\mathbf{d}_{\text{ext.}}^T\mathbf{s} &= d_{\text{ext.}_1}s_1 + \cdots + d_{\text{ext.}_n}s_n, \\
&\le |d_{\text{ext.}_1}||s_1| + \cdots + |d_{\text{ext.}_n}||s_n|, \\
&\le |\mathbf{d}_{\text{ext.}}^T||\mathbf{s}|, \\
&\le \mathbf{D}_{\text{ext.}}^T|\mathbf{s}|,
\end{aligned}$$

and

$$\begin{aligned}
\mathbf{d}_{\text{in.}}^T\mathbf{s} &= d_{\text{in.}_1}s_1 + \cdots + d_{\text{in.}_n}s_n, \\
&\le |d_{\text{in.}_1}||s_1| + \cdots + |d_{\text{in.}_n}||s_n|, \\
&\le |\mathbf{d}_{\text{in.}}^T||\mathbf{s}|.
\end{aligned}$$

https://doi.org/10.1017/S0263574714000332 Published online by Cambridge University Press